Ohyama K, Yasuda K, Onga K, Kakizuka A, Mori N.	Spatio- temporal expression pattern of the NatB complex, Nat5/Mdm20 in the developing mouse brain: implications for co-operative versus non-co-operative actions of Mdm20 and Nat5.	Gene Expr Patterns	12	36-45	2012
Muraoka Y, Ohashi-Ikeda H, Nakano N, Hangai M, Toda Y, Okamoto-Furuta K, Kohda H, Kondo M, Terasaki H, Kakizuka A, Yoshimura N.	Real-Time Imaging of Rabbit Retina with Retinal Degeneration by using Spectral-Domain Optical Coherence Tomography.	PLoS ONE	7	e36135	2012
Takata T, Kimura Y, Ohnuma Y, Kawawaki J, Kakiyama S, Tanaka K, Kakizuka A.	Rescue of growth defects of yeast *cdc48* mutants by pathogenic IBMPFD-VCPs.	J. Str. Biol.	173	93-103	2012
Sakurai H, Sakaguchi Y, Shoji E, Nishino T, Maki I, Sakai H, Hanaoka K, Kakizuka A, Sehara-Fujisawa A.	In vitro modeling of paraxial mesodermal progenitors derived from induced pluripotent stem cells.	PLoS ONE	7	e47078	2012
Murakami K, Ichinohe Y, Koike M, Sasaoka N, Iemura S, Natsume T, Kakizuka A.	VCP Is an Integral Component of a Novel Feedback Mechanism that Controls Intracellular Localization of Catalase and H_2O_2 Levels.	PLoS ONE	8	e56012	2013

Sasaoka N, Sakamoto M, Kanemori S, Tsukano C, Takemoto Y, Kakizuka A.	Tsukano C, Takemoto Y, & Kakizuka A. Long-term oral administration of Hop flower extracts mitigates Alzheimer phenotypes in mice.	submitted			2013

III. 研究成果の刊行物・別刷

Biochemical and Biophysical Research Communications 394 (2010) 42–47

Contents lists available at ScienceDirect

Biochemical and Biophysical Research Communications

journal homepage: www.elsevier.com/locate/ybbrc

Maintaining ATP levels via the suppression of PERK-mediated rRNA synthesis at ER stress

Akihiko Okamoto, Masaaki Koike, Kunihiko Yasuda, Akira Kakizuka *

The Laboratory of Functional Biology, Kyoto University Graduate School of Biostudies/SORST (JST), Kyoto 606-8501, Japan

ARTICLE INFO

Article history:
Received 26 January 2010
Available online 19 February 2010

Keywords:
eIF2α phosphorylation
ER stress
PERK
Protein synthesis suppression
rRNA synthesis suppression

ABSTRACT

Currently, [^{3}H]uridine is most often used to monitor rRNA synthesis in cultured cells. We show here that radiolabeled ribonucleoside triphosphates, such as [α-^{33}P]UTP, in culture medium were also incorporated efficiently not only into cells but also into *de novo* RNA, particularly rRNA. Using this method, we first revealed that endoplasmic reticulum (ER) stress inducers such as tunicamycin and thapsigargin suppressed *de novo* rRNA synthesis, and that PERK, but not IRE1α or ATF6, mediated the suppression. PERK is known to mediate the suppression of *de novo* protein synthesis via phosphorylation of eIF2α. Consistently, other translational inhibitors such as PSI, proteasomal inhibitor, and cycloheximide suppressed *de novo* rRNA synthesis. eIF2α knockdown also suppressed both *de novo* protein and rRNA syntheses. Furthermore, ER stress reduced cellular ATP levels, and the suppression of rRNA synthesis apparently mitigated their reduction. These observations provided a close link between ATP levels and suppression of *de novo* rRNA synthesis at ER stress, and we proposed a novel feedback mechanism, in which ATP levels were maintained via suppression of *de novo* rRNA synthesis in ATP-demanding stresses, such as ER stress.

Feedback mechanisms are the core machinery for organisms and cells to remain healthy in the face of changes in the environment. In cellular levels, unfolded protein response (UPR) in endoplasmic reticulum (ER) provides good examples of "feedback mechanisms" [1,2]. ER is an intracellular organelle, in which membrane and secreted proteins are properly folded and modified. When proteins that pass through the ER are not correctly modified or folded, such misfolded proteins are easily accumulated in the ER [3,4]. The accumulation of misfolded proteins triggers several cellular responses, including transcriptional induction of chaperons, stimulation of ER-associated degradation (ERAD) [5], and translational inhibition of mRNAs [6,7]. These responses are collectively called UPR, and all aim to reduce the amounts of accumulated misfolded proteins in the ER [2]. In general, translational inhibition apparently occurs at the earliest time point during UPR, followed by the induction of chaperons and stimulation of ERAD, and thus the translational inhibition, namely suppression of *de novo* protein synthesis, might be a primary demand for cells in handling ER stress.

In UPR, ATF6, IRE1α, and PERK have been shown to function as sensor proteins [6,8–10], which are able to recognize the accumulation of misfolded proteins in the ER, and after the recognition, these proteins trigger signaling cascades for the UPR. Among the three, PERK, a PKR-like kinase, is known to mediate translational inhibition [6]. When PERK is activated at ER stress, activated PERK mediates phosphorylation of Ser51 of the alpha subunit of eukaryotic translation initiation factor (eIF2α), which in turn leads to translational inhibition [6,7]. This provides an elegant feedback system, which prevents further supply of misfolded proteins in the ER. It is noteworthy that the Ser51 phosphorylation of eIF2α has also been observed in several other stress conditions, such as virus infection, oxidative stress, ultraviolet exposure, amino-acid starvation, etc. [11–14]. However, in some of these stress conditions, there seems to be no need of suppression of *de novo* protein synthesis as a feedback mechanism. Thus, yet unknown meaning of the suppression of *de novo* protein synthesis in these stress conditions, including ER stress, might exist.

ATP is necessary in essentially all cellular activities, and its needs increase in stress conditions such as ER stress, in which chaperons utilize ATP in unfolding [15], VCP in ERAD [16,17], proteasome in the degradation of misfolded proteins [18]. Ubiquitination also utilizes ATP for marking unnecessary proteins to be degraded [19]. ATP levels are maintained in the balance between its synthesis and consumption. Although basic mechanism for ATP production by F1F0 ATPase and its consumption by other ATPases are well documented, regulatory mechanisms in keeping ATP levels are only poorly understood [20]. It is noteworthy that large amounts of ATP are also consumed in RNA synthesis, especially in ribosomal RNA (rRNA) synthesis [21]. In this study, we report profound couplings among ATP-demanding conditions, translational

* Corresponding author. Fax: +81 75 753 7676.
E-mail address: kakizuka@lif.kyoto-u.ac.jp (A. Kakizuka).

0006-291X/$ - see front matter © 2010 Elsevier Inc. All rights reserved.
doi:10.1016/j.bbrc.2010.02.065

inhibition, and suppression of *de novo* rRNA synthesis, and propose a novel feedback mechanism.

Materials and methods

Antibodies. Anti-CBP, anti-UBF, anti-TIF-IA, and anti-c-myc antibodies were purchased from Santa Cruz. Anti-eIF2α antibodies were purchased from Cell Signaling. An anti-actin antibody was purchased from Chemicon. An anti-ATF6 antibody was a gift from Dr. Kazutoshi Mori.

Cell Culture. HeLa cells were cultured in Dulbecco's modified Eagle's medium (DMEM) with 10% fetal bovine serum and penicillin and streptomycin. Indicated amounts of tunicamycin (Nacalai Tesque), Thapsigargin (Nacalai Tesque), PSI (Peptide Institute), Actinomycin D (Nacalai Tesque), and α-amanitin (Invitrogen) were added 2 h prior to the addition of [α-^{33}P]UTP to the medium.

Visualization of rRNA synthesis (VRS). When cells grew at 70–80% confluency, 20 μCi [α-^{33}P]UTP (3000 Ci/mmol) (GE Helthcare) was added to the culture medium. Total RNA was isolated by the acid guanidine phenol chloroform method using Trizol Reagent (Invitrogen). Five micrograms of total RNA was separated in 1% agarose gel, and then transferred onto a nylon membrane (Hybond-N+ membrane) (GE Healthcare). Dried membranes were subjected to autoradiography.

RNAi experiments. Sequences of siRNAs used in this study are listed in Supplementary Table 1. HeLa cells (3×10^5) were transfected with 25 nM siRNAs using Oligofectamine (Invitrogen), and were cultured for 3 days. Cells were then cultured for 2 h in the absence or presence of chemicals, followed by the additional 8 h culture with [α-^{33}P]UTP in the absence or presence of chemicals, respectively, and then total RNA was recovered and analyzed.

Measurement of de novo protein synthesis. HeLa cells (3×10^5) were cultured with methionine- and cysteine-free DMEM containing 10% FBS for 30 min. Then, 25 μCi [^{35}S]methionine/cysteine (37 TBq/mmol) (GE Healthcare) were added to the medium for 30 min. Then cells were washed with ice-cold PBS three times and lysed with RIPA buffer. After centrifugation at 15,000 rpm for 30 min at 4 °C, the supernatants were collected and their protein concentrations were determined. Ten micrograms of lysates was separated by SDS–PAGE, and the gel was fixed with methanol. Then the gel was dried and exposed onto an X-ray film (Fuji film). Alternatively, their radioactivity was determined with a liquid scintillation counter.

Measurement of ATP in cultured cells. ATP was measured by luciferase activities by ARVO multilabel counter (Wallac), using Cellno ATP assay reagent (Toyo B-net Co., Ltd.).

Establishment of HeLa cells expressing eIF2α. A full-length human eIF2α cDNA (No. NM_004094) was obtained from RIKEN BRC DNA BANK [22]. Using a lenti virus system, HeLa cells continuously expressing eIF2α were established. These cells, but not normal HeLa cells, allowed the eIF2α phosphorylation to be detected by Western blot.

Statistical analysis. Each experiment was conducted at least three times with consistent results. The representative gel or blot from each experiment is presented in this study. Mean values and standard deviations were obtained from triplicate experiments.

Results

Visualization of rRNA synthesis

It is generally thought that ribonucleoside triphosphates cannot pass through the plasma membrane due to their hydrophilic or water-soluble nature [23], and thus that it is impossible to radiolabel newly synthesized rRNA in cultured cells by adding radiolabeled ribonucleoside triphosphates, such as [α-^{33}P]UTP, to the culture medium. In contrast, [^{3}H]uridine, a more hydrophobic and smaller molecule than UTP, has been shown to pass through the plasma membrane, and thus it has been used to radiolabel the RNA in many experiments using cultured cells [24]. We cultured a variety of cell lines (HeLa, HEK293A, HEK293T, CV-1, COS1, COS7, PC12, etc.), added 20 μCi [α-^{33}P]UTP (3000 Ci/mmol) to 2 ml of culture medium, incubated for 8 h, harvested the cells, and recovered the RNA. Surprisingly, RNAs from all of the cells exhibited radioactivity. Among the cell lines, RNA from HeLa cells was the most highly radioactive, indicating that UTP was being efficiently incorporated. To the best of our knowledge, this simple method allowed to radiolabel the RNA in cultured cells, for the first time, by using a radiolabeled ribonucleoside triphosphate, namely [α-^{33}P]UTP, although molecular basis as to how UTP passes through the plasma membrane remains to be clarified. [α-^{33}P]UTP contains [^{33}P], a high-energy radioisotope, and thus newly synthesized RNA was expected to be detected much more easily by autoradiography than using [^{3}H]uridine.

We then pulse-labeled HeLa cells for 30 min and analyzed the RNA by agarose gel electrophoresis, followed by membrane transfer and autoradiography. [α-^{33}P]UTP was first incorporated into rRNA precursors and then shifted to mature 28S, 18S, and 5.8S rRNAs in a time-dependent manner (Fig. 1A). Although mRNA could also be visualized as smears in the gel after long periods of labeling, after 30 min of labeling, the several bands predominated at the expected positions for pre-rRNA and mature rRNA (Fig. 1A). These bands were destroyed by RNase A treatment, but not by DNase I treatment (data not shown). Incorporation of [α-^{33}P]UTP into the RNA in these bands was consistently suppressed by addition of actinomycin D (ActD), an inhibitor of RNA polymerase I, but not α-amanitin, an inhibitor of RNA polymerase II to the culture medium (Fig. 1B).

ER stress suppressed rRNA synthesis

We then searched for stressors or compounds that affected rRNA synthesis, and found that tunicamycin (Tm), thapsigargin (Tg), and proteasome inhibitor (PSI) treatments efficiently suppressed *de novo* rRNA labeling (Fig. 1C). Under the same conditions, c-myc levels were slightly decreased by Tm treatment, but were not affected by Tg or PSI treatment (Fig. 1D). c-myc has been shown to increase rRNA synthesis [24]. However, Tm, Tg, and PSI are known to induce endoplasmic reticulum stress (ER stress). Indeed, these three compounds induced CHOP expression, a well-known ER stress marker (Fig. 1D) [25]. We thus hypothesized that ER stress could induce the suppression of *de novo* rRNA synthesis.

We pulse-labeled cells with or without Tm treatment, and examined the profile of rRNA synthesis suppression. Tm treatment did not appear to change the pattern of the bands labeled by [α-^{33}P]UTP, but the strength of each band was greatly reduced (Fig. 1E). Treatment with Tg or PSI produced results that were essentially identical to those observed in Tm treatment (data not shown). We further examined the effects of these compounds after incorporated [α-^{33}P]UTP had shifted completely into mature 28S and 18S rRNA, and found that none of the compounds affected the incorporated [α-^{33}P]UTP patterns in mature 28S or 18S rRNA (Fig. 1F). These results demonstrate that the rRNA transcription was suppressed by Tm treatment, and that maturation or degradation of rRNA did not appear to be affected by Tm treatment.

PERK-mediated rRNA synthesis suppression at ER stress

To obtain more evidence in support of the idea that ER stress induces rRNA synthesis suppression, we examined the effect of blockading the major ER stress signaling pathways, namely, IRE1α,

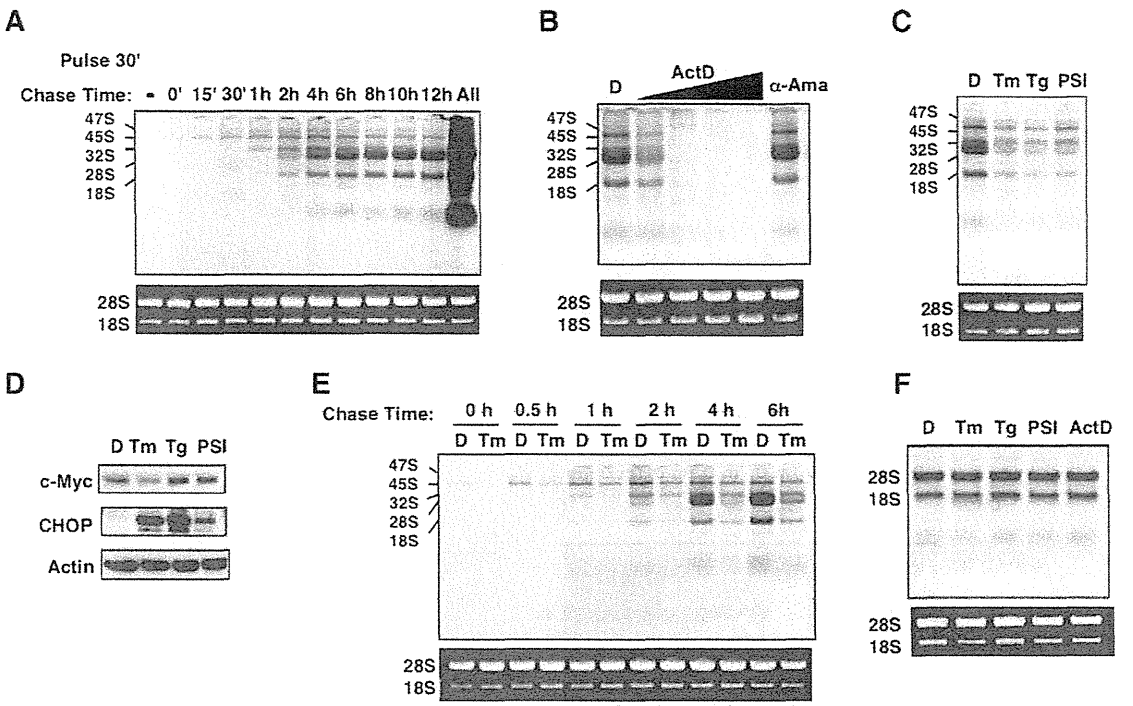

Fig. 1. Visualization of *de novo* rRNA synthesis and its suppression following ER stress. (A) HeLa cells were labeled with [α-^{33}P]UTP for 30 min or 12.5 h (All). Following the 30 min labeling, cells were washed, and cultured for the indicated time periods (from 0 to 12 h). Newly synthesized RNA was detected, as described in "Materials and methods". rRNA patterns are shown as a loading control. (B) HeLa cells were cultured for 8 h with 20 μCi of [α-^{33}P]UTP in the absence (D) or presence of ActD (1, 10, 100, or 1000 μg/ml) or α-amanitin (α-Ama) (50 nM). RNA was then recovered and analyzed as described in (A). (C) HeLa cells were cultured for 2 h in the absence (D) or presence of Tm (2 μg/ml), Tg (500 nM), or PSI (10 μM). RNA was radiolabeled and analyzed as described in (A). (D) HeLa cells were cultured for 8 h in the absence (D) or presence of Tm (2 μg/ml), Tg (500 nM), or PSI (10 μM), and the cell lysates were analyzed by western blot using anti-c-myc, anti-CHOP, and anti-actin antibodies. (E) HeLa cells were cultured for 2 h in the absence (D) or presence of 2 μg/ml Tm, and then 20 μCi of [α-^{33}P]UTP was added to the medium for 30 min. After extensive washing, cells were cultured for the indicated additional time periods (from 0 to 6 h), and RNA was recovered and analyzed as described in (A). (F) HeLa cells were cultured for 3 h with 20 μCi of [α-^{33}P]UTP. Twenty-four hours after the medium change, cells were cultured for an additional 8 h in the absence (D) or presence of Tm (2 μg/ml), Tg (500 nM), or PSI (10 μM). RNA was recovered and analyzed as described in (A).

ATF6, and PERK pathways [6,8,9]. Neither of the two different IRE1α siRNAs inhibited the suppression of rRNA synthesis by Tm (Fig. 2A and Supplementary Fig. S1). Consistent with this, we could not detect inhibition of rRNA synthesis suppression in MEF from IRE1α (−/−) mice (Supplementary Fig. S2). Furthermore, neither of the two different ATF6 siRNAs inhibited the rRNA synthesis suppression (Fig. 2A), although both ATF6 siRNAs efficiently reduced endogenous ATF6 protein levels (Fig. 2B). However, four different PERK siRNAs did inhibit the suppression of rRNA synthesis by Tm (Fig. 2A), although all of the PERK siRNAs effectively destroyed PERK mRNA (Supplementary Fig. S3). Indeed, in the cells treated with PERK siRNAs, induction of CHOP by Tm was inhibited (Fig. 2B). We could rule out the involvement of CHOP in rRNA synthesis suppression, because we observed clear suppression of rRNA synthesis in MEF from CHOP (−/−) mice (Fig. 2C) [26]. PERK siRNAs also induced a similar inhibition of rRNA synthesis suppression in cells treated with Tg, but not in those treated with PSI (Fig. 2D), suggesting that, in addition to PERK, other as-yet unknown molecule(s) may be involved in suppressing *de novo* rRNA synthesis when misfolded proteins or ubiquitinated proteins accumulate in the cytoplasm, as observed after PSI treatment.

Translational inhibition and rRNA synthesis suppression

During UPR, PERK is involved in the translational inhibition of mRNA via eIF2α phosphorylation at Ser51 [7], in addition to the induction of CHOP [25]. Thus, we next examined the possible involvement of translational inhibition in the suppression of rRNA synthesis. Indeed, we observed that 10 μg/ml cycloheximide (CHX) treatment caused the suppression of not only *de novo* protein synthesis but also rRNA synthesis. Both suppressions were not dependent of PERK (Fig. 3A and B). Although CHX treatment slightly induced eIF2α phosphorylation, it was not PERK-dependent (Fig. 3C). Likewise, PSI treatment caused not only suppression of *de novo* protein synthesis but also eIF2α phosphorylation (Fig. 3A and C), which appeared to be partly dependent on PERK (Fig. 3C). Furthermore, two eIF2α siRNAs markedly suppressed *de novo* protein and rRNA syntheses (Fig. 3D and E, and Supplementary Fig. S4). In cells treated with eIF2α siRNAs, Tm was not able to further enhance the suppression of *de novo* protein or rRNA synthesis (Fig. 3D and E). These data, altogether, indicated that suppression of *de novo* protein synthesis profoundly couples with the suppression of *de novo* rRNA synthesis.

Suppression of rRNA synthesis apparently contributed to maintaining ATP levels

We observed that 10 ng/ml ActD showed slightly stronger suppressive effect on *de novo* rRNA synthesis than 2 μg/ml Tm (Fig. 3B), and this concentration of Tm suppressed more than 60% of *de novo* protein synthesis. However, this dose of ActD only marginally suppressed *de novo* protein synthesis for up to 24 h (Fig. 4A). These results indicate that the observed suppression of *de novo* rRNA synthesis affected *de novo* protein synthesis very mildly. How, then, does suppression of *de novo* rRNA synthesis benefit cells with large accumulations of misfolded proteins in

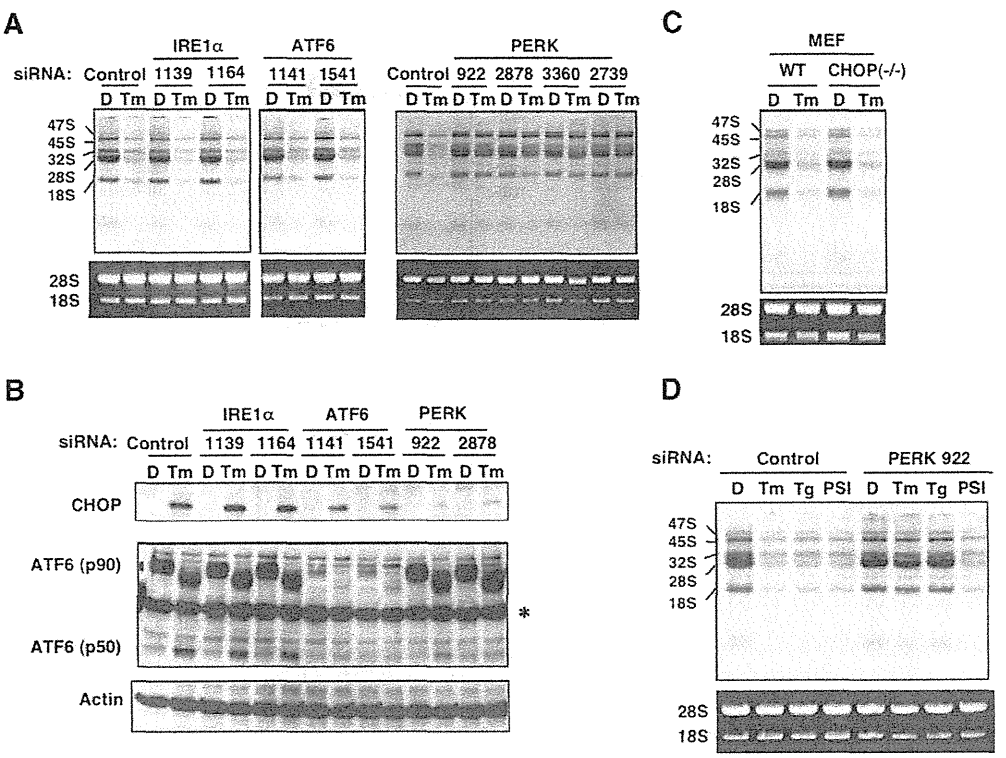

Fig. 2. PERK mediates ER stress-induced suppression of *de novo* rRNA synthesis. (A, C, D) HeLa cells were transfected with indicated siRNAs, and cultured for 3 days. Cells were then cultured for 2 h in the absence (D) or presence of Tm (2 μg/ml), and 20 μCi of [α-^{33}P]UTP was added to the medium. Cells were cultured for an additional 8 h, and RNA was recovered and analyzed as described in Fig. 1A. (B) HeLa cells were transfected with indicated siRNAs and cultured for 3 days. Cells were then cultured for 8 h in the absence (D) or presence of Tm (2 μg/ml), and the cell lysates were analyzed by western blot using anti-CHOP, anti-ATF6, and anti-actin antibodies. * indicates nonspecific bands. (C) MEF cells from wild-type mice (WT) or from CHOP knockout mice (CHOP (−/−)) were cultured for 2 h in the absence (D) or presence of Tm (2 μg/ml). RNA was radiolabeled and analyzed as described in Fig. 1A. (D) HeLa cells were transfected with PERK siRNA (922), and cultured for 3 days. Cells were then cultured for 2 h in the absence (D) or presence of Tm (2 μg/ml), Tg (500 nM), or PSI (10 μM). RNA was radiolabeled and analyzed as described in Fig. 1A.

the ER (at ER stress) or in the cytoplasm (at PSI treatment)? Large amounts of ATP are consumed continuously during rRNA synthesis [21]. In these cells, ATP is required by chaperons and the ubiquitin–proteasome system for unfolding and ubiquitination-degradation, respectively, of the accumulated proteins [5]. Thus, the observed suppression of *de novo* rRNA synthesis likely maintains the supply of ATP in these cells by reducing the consumption of ATP for rRNA synthesis so that it can be used instead to power chaperons and the ubiquitin–proteasome system. We then examined this possibility. Tm treatment indeed reduced ATP levels in the cells, and this reduction was further enhanced with PERK knockdown (Fig. 4B). Furthermore, addition of ActD significantly recovered ATP levels in cells treated with Tm but not in cells cultured in a normal condition (Fig. 4B).

Discussions

In this study, we first showed a novel method to analyze *de novo* RNA synthesis, especially rRNA synthesis, in cultured cells by simply adding radiolabeled ribonucleoside triphosphate, such as [α-^{33}P]UTP in culture medium, followed by RNA extraction, gel electrophoresis, RNA blotting, and autoradiography. This simple method allows to visualize entire steps of rRNA synthesis, e.g. precursor transcription of 47S rRNA, processing, and appearance of mature 18S and 28S rRNA, in a quantitative manner. Thus, we call this method VRS (visualization of RNA synthesis) method.

Using VRS method, we next revealed that ER stress-inducing drugs, such as Tm, Tg, and PSI dramatically suppressed *de novo* rRNA synthesis. It has been reported that ER stress induces various cellular responses via using ER stress sensors, such as ATF6, PERK, IRE1α [6,8,9]. Among the knockdown of these three sensors, only PERK knockdown abolished Tm- and Tg-mediated but not PSI-mediated suppression of rRNA synthesis. These observations evidenced that PERK is involved in the suppression of rRNA synthesis at ER stress. PERK has been known to phosphorylate Ser51 in eIF2α, which in turn causes translational inhibition. Consistently, PSI induced the phosphorylation of Ser51 in eIF2α, even in cells treated with PERK siRNAs. Thus, the suppression of rRNA synthesis observed apparently coupled with the eIF2α phosphorylation.

Recently, DuRose et al. showed very similar observations and suggested that eIF2α phosphorylation couples with RRN3/TIF-IA being released from RNA polymerase I at ER stress, leading to the suppression of rRNA synthesis [27]. They speculated that RRN3/TIF-IA phosphorylation might be responsible for the release [27]. In our experiments, RRN3/TIF-IA knockdown was indeed able to suppress the rRNA synthesis (Supplementary Fig. S5). However, knockdown of eIF2α also induced similar suppression of rRNA synthesis in concomitant with the suppression of *de novo* protein synthesis, indicating that eIF2α phosphorylation is not necessary for the suppression of rRNA synthesis. Furthermore, CHX treatment was able to strongly suppress both protein and rRNA syntheses. These observations could provide an alternative, but not necessarily a mutually exclusive mechanism of the suppression of rRNA synthesis. Namely, translational suppression itself is responsible for the suppression of rRNA synthesis. In this mechanism, it is

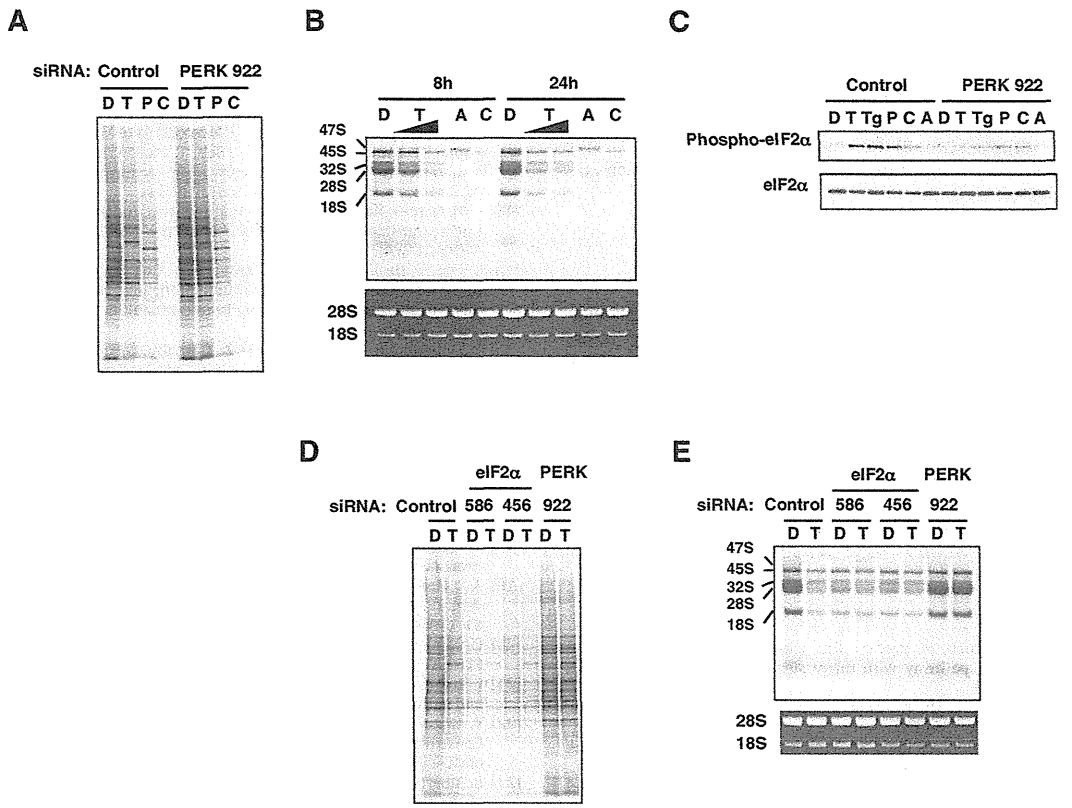

Fig. 3. Translational inhibition and the suppression of rRNA synthesis. (A and D) Measurements of *de novo* protein synthesis (see "Materials and methods") in the absence (D) or presence of Tm (T) (2 μg/ml), PSI (P) (10 μM), CHX (C) (10 μg/ml) for 8 h from cells treated with indicated siRNAs. (B and E) HeLa cells were transfected with indicated siRNAs and cultured for 3 days. Cells were then cultured for 8 h in the absence (D) or presence of Tm (T) (0.2 or 2 μg/ml), PSI (P) (10 μM), ActD (A) (10 ng/ml), and CHX (C) (10 μg/ml). RNA was radiolabeled and analyzed as described in Fig. 1A. (C) Western blot analysis using anti-phospho eIF2α and eIF2α antibodies on cell lysates from HeLa cells overexpressing eIF2α. Cells were transfected with PERK siRNA (922), and cultured for 3 days. Cells were then cultured for 2 h in the absence (D) or presence of Tm (T) (2 μg/ml), Tg (500 nM), PSI (P) (10 μM), CHX (C) (10 μg/ml), and ActD (A) (10 ng/ml).

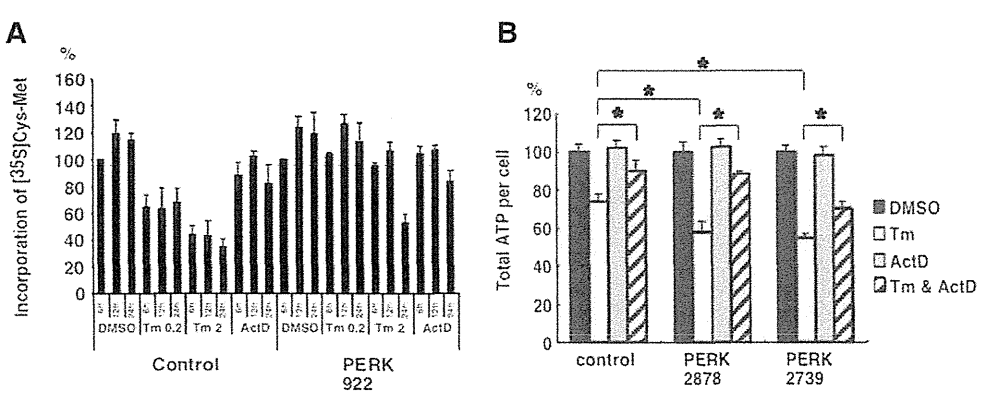

Fig. 4. Suppression of rRNA synthesis and ATP levels at ER stress. (A) Measurements of the relative amounts of *de novo* protein synthesis (see "Materials and methods") in the absence (DMSO) and presence of Tm (0.2, or 2 μg/ml) and ActD (10 ng/ml) for 6, 12 or 24 h. (B) Measurements of the relative amounts of ATP per cell. HeLa cells were treated in the absence (DMSO) and presence of Tm (2 μg/ml), ActD (10 ng/ml), or both for 24 h, and were harvested. Then, ATP amounts from 1.5×10^5 cells were measured (see "Materials and methods"). *, $p < 0.05$.

speculated that protein(s) with very short half-lives or those that are quickly ubiquitinated would play important roles in rRNA synthesis. These possibilities remain to be clarified.

It was evident that simple suppression of rRNA synthesis by ActD did not appear to contribute to the suppression of *de novo* protein synthesis. Instead, the observed suppression of *de novo* rRNA synthesis maintained the ATP levels in cells with ER stress by reducing the consumption of ATP for rRNA synthesis so that it can be used by other systems, such as ER chaperons, ERAD, and the ubiquitin–proteasome system. It is noteworthy that eIF2α phosphorylation occurs not only at ER stress, but also in several other stress conditions, such as amino-acid starvation, oxidative

stress, virus infection, etc. [11–14]. These conditions apparently all require large amounts of ATP, and thus the cells use eIF2α phosphorylation to suppress the supply of newly synthesized proteins, which in turn suppresses the *de novo* rRNA synthesis, leading to the maintenance of ATP levels in the cell. Thus, this system would be a fundamental feedback system for the cells to adapt or survive against several stressful conditions via efficiently utilizing intracellular pools of ATP.

Acknowledgments

We wish to thank professors Kenji Kohno (Nara Institute of Science and Technology), Shizuo Akira (Osaka University), Kazutoshi Mori (Kyoto University), and RIKEN BRC DNA Bank for IRE1α knockout MEF, CHOP knockout MEF, an anti-ATF6 antibody, and pAxCALNLheIF2α, respectively.

Appendix A. Supplementary data

Supplementary data associated with this article can be found, in the online version, at doi:10.1016/j.bbrc.2010.02.065.

References

[1] C. Sidrauski, R. Chapman, P. Walter, The unfolded protein response: an intracellular signalling pathway with many surprising features, Trends Cell Biol. 8 (1998) 245–249.
[2] M. Schroder, R.J. Kaufman, The mammalian unfolded protein response, Annu. Rev. Biochem. 74 (2005) 739–789.
[3] R.B. Freedman, A.D. Dunn, L.W. Ruddock, Protein folding: a missing redox link in the endoplasmic reticulum, Curr. Biol. 8 (1998) R468–R470.
[4] A.R. Frand, J.W. Cuozzo, C.A. Kaiser, Pathways for protein disulphide bond formation, Trends Cell Biol. 10 (2000) 203–210.
[5] A. Ahner, J.L. Brodsky, Checkpoints in ER-associated degradation: excuse me, which way to the proteasome?, Trends Cell Biol 14 (2004) 474–478.
[6] H.P. Harding, Y. Zhang, D. Ron, Protein translation and folding are coupled by an endoplasmic-reticulum-resident kinase, Nature 397 (1999) 271–274.
[7] H.P. Harding, Y. Zhang, A. Bertolotti, H. Zeng, D. Ron, Perk is essential for translational regulation and cell survival during the unfolded protein response, Mol. Cell 5 (2000) 897–904.
[8] H. Yoshida, K. Haze, H. Yanagi, T. Yura, K. Mori, Identification of the cis-acting endoplasmic reticulum stress response element responsible for transcriptional induction of mammalian glucose-regulated proteins. Involvement of basic leucine zipper transcription factors, J. Biol. Chem. 273 (1998) 33741–33749.
[9] X.Z. Wang, H.P. Harding, Y. Zhang, E.M. Jolicoeur, M. Kuroda, D. Ron, Cloning of mammalian Ire1 reveals diversity in the ER stress responses, EMBO J. 17 (1998) 5708–5717.
[10] H. Yoshida, T. Matsui, A. Yamamoto, T. Okada, K. Mori, XBP1 mRNA is induced by ATF6 and spliced by IRE1 in response to ER stress to produce a highly active transcription factor, Cell 107 (2001) 881–891.
[11] M. Gale Jr., M.G. Katze, Molecular mechanisms of interferon resistance mediated by viral-directed inhibition of PKR, the interferon-induced protein kinase, Pharmacol. Ther. 78 (1998) 29–46.
[12] H.P. Harding, Y. Zhang, H. Zeng, I. Novoa, P.D. Lu, M. Calfon, N. Sadri, C. Yun, B. Popko, R. Paules, D.F. Stojdl, J.C. Bell, T. Hettmann, J.M. Leiden, D. Ron, An integrated stress response regulates amino acid metabolism and resistance to oxidative stress, Mol. Cell 11 (2003) 619–633.
[13] K.M. Vattem, R.C. Wek, Reinitiation involving upstream ORFs regulates ATF4 mRNA translation in mammalian cells, Proc. Natl. Acad. Sci. USA 101 (2004) 11269–11274.
[14] S. Wu, Y. Hu, J.L. Wang, M. Chatterjee, Y. Shi, R.J. Kaufman, Ultraviolet light inhibits translation through activation of the unfolded protein response kinase PERK in the lumen of the endoplasmic reticulum, J. Biol. Chem. 277 (2002) 18077–18083.
[15] P. Goloubinoff, J.T. Christeller, A.A. Gatenby, G.H. Lorimer, Reconstitution of active dimeric ribulose bisphosphate carboxylase from an unfolded state depends on two chaperonin proteins and Mg-ATP, Nature 342 (1989) 884–889.
[16] T. Kobayashi, K. Tanaka, K. Inoue, A. Kakizuka, Functional ATPase activity of p97/valosin-containing protein (VCP) is required for the quality control of endoplasmic reticulum in neuronally differentiated mammalian PC12 cells, J. Biol. Chem. 277 (2002) 47358–47365.
[17] P.D. Lu, H.P. Harding, D. Ron, Translation reinitiation at alternative open reading frames regulates gene expression in an integrated stress response, J. Cell Biol. 167 (2004) 27–33.
[18] T. Ogura, K. Tanaka, Dissecting various ATP-dependent steps involved in proteasomal degradation, Mol. Cell 11 (2003) 3–5.
[19] A. Hershko, E. Leshinsky, D. Ganoth, H. Heller, ATP-dependent degradation of ubiquitin-protein conjugates, Proc. Natl. Acad. Sci. USA 81 (1984) 1619–1623.
[20] C. von Ballmoos, A. Wiedenmann, P. Dimroth, Essentials for ATP synthesis by F1F0 ATP synthases, Annu. Rev. Biochem. 78 (2009) 649–672.
[21] J. Russell, J.C. Zomerdijk, RNA-polymerase-I-directed rDNA transcription, life and works, Trends Biochem. Sci. 30 (2005) 87–96.
[22] Y. Suzuki, K. Yoshitomo-Nakagawa, K. Maruyama, A. Suyama, S. Sugano, Construction and characterization of a full length-enriched and a 5′-end-enriched cDNA library, Gene 200 (1997) 149–156.
[23] B. Alberts, A. Johnson, J. Lewis, M. Raff, K. Roberts, P. Walter, Molecular Biology of the Cell, Fifth ed., Garland Science, New York, 2008. pp. 652–653.
[24] C. Grandori, N. Gomez-Roman, Z.A. Felton-Edkins, C. Ngouenet, D.A. Galloway, R.N. Eisenman, R.J. White, c-Myc binds to human ribosomal DNA and stimulates transcription of rRNA genes by RNA polymerase I, Nat. Cell Biol. 7 (2005) 311–318.
[25] X.Z. Wang, B. Lawson, J.W. Brewer, H. Zinszner, A. Sanjay, L.J. Mi, R. Boorstein, G. Kreibich, L.M. Hendershot, D. Ron, Signals from the stressed endoplasmic reticulum induce C/EBP-homologous protein (CHOP/GADD153), Mol. Cell. Biol. 16 (1996) 4273–4280.
[26] S. Oyadomari, K. Takeda, M. Takiguchi, T. Gotoh, M. Matsumoto, I. Wada, S. Akira, E. Araki, M. Mori, Nitric oxide-induced apoptosis in pancreatic beta cells is mediated by the endoplasmic reticulum stress pathway, Proc. Natl. Acad. Sci. USA 98 (2001) 10845–10850.
[27] J.B. DuRose, D. Scheuner, R.J. Kaufman, L.I. Rothblum, M. Niwa, Phosphorylation of eukaryotic translation initiation factor 2alpha coordinates rRNA transcription and translation inhibition during endoplasmic reticulum stress, Mol. Cell. Biol. 29 (2009) 4295–4307.

THE JOURNAL OF BIOLOGICAL CHEMISTRY VOL. 285, NO. 28, pp. 21736–21749, July 9, 2010

Valosin-containing Protein (VCP) in Novel Feedback Machinery between Abnormal Protein Accumulation and Transcriptional Suppression*[S]

Received for publication, December 29, 2009, and in revised form, March 31, 2010 Published, JBC Papers in Press, April 21, 2010, DOI 10.1074/jbc.M109.099283

Masaaki Koike[‡], Junpei Fukushi[‡], Yuzuru Ichinohe[‡], Naoki Higashimae[‡], Masahiko Fujishiro[‡], Chiyomi Sasaki[‡], Masahiro Yamaguchi[§], Toshiki Uchihara[¶], Saburo Yagishita[‖], Hiroshi Ohizumi[‡], Seiji Hori[‡], and Akira Kakizuka[‡1]

From the [‡]Laboratory of Functional Biology, Kyoto University Graduate School of Biostudies & Solution Oriented Research for Science and Technology (JST), Kyoto 606-8501, Japan, the [§]Department of Physiology, Graduate School of Medicine, The University of Tokyo, Tokyo 113-0033, Japan, the [¶]Department of Neurology, Tokyo Metropolitan Institute for Neuroscience, Tokyo 183-8526, Japan, and the [‖]Department of Pathology, Kanagawa Rehabilitation Center, Kanagawa 243-0121, Japan

Abnormal protein accumulation is often observed in human neurodegenerative disorders such as polyglutamine diseases and Parkinson disease. Genetic and biochemical analyses indicate that valosin-containing protein (VCP) is a crucial molecule in the pathogenesis of human neurodegenerative disorders. We report here that VCP was specifically modified in neuronal cells with abnormal protein accumulation; this modification caused the translocation of VCP into the nucleus. Modification-mimic forms of VCP induced transcriptional suppression with deacetylation of core histones, leading to cell atrophy and the decrease of *de novo* protein synthesis. Preventing VCP nuclear translocation in polyglutamine-expressing neuronal cells and *Drosophila* eyes mitigated neurite retraction and eye degenerations, respectively, concomitant with the recovery of core histone acetylation. This represents a novel feedback mechanism that regulates abnormal protein levels in the cytoplasm during physiological processes, as well as in pathological conditions such as abnormal protein accumulation in neurodegenerations.

Homeostasis is a fundamental property of organisms and cells that allows them to remain healthy in the face of changes in the environment. Feedback mechanisms are the core machinery for maintaining homeostasis. One example of feedback mechanism is end-product inhibition in enzyme reactions, and another is unfolded protein response (UPR)[2] in ER (1, 2). The goal of UPR is to reduce the amount of accumulated misfolded proteins in the ER (3). Although there have been a number of studies of the elegant feedback mechanisms employed for ER quality control, it is currently unknown whether similar mechanisms exist to reduce the cytoplasmic accumulation of misfolded proteins. Many neurodegenerative diseases (*e.g.* polyglutamine diseases, AD, PD, and ALS) share pathological features such as accumulation of abnormal proteins, neural cell atrophy, or degeneration, and neuronal cell death (4, 5), suggesting that common molecular mechanisms underlie these disorders. Indeed polyglutamine expansions have been identified in aggregated proteins in nine inherited neurodegenerative disorders, including HD and MJD (also called SCA3), α-synuclein in PD, DLB, and multisystem atrophy, and TDP-43 in certain types of front-temporal dementia, PD without Lewy bodies, and ALS (4–6). These proteins accumulate in the cytoplasm, the nucleus, or both, and have been proposed to trigger multiple cellular responses, such as cell death, proteasomal dysfunction, ER stress, and oxidative stress (7–11), as well as transcriptional dysregulation (12, 13).

Transcriptional regulation of gene expression is often accompanied by histone modifications, such as acetylation, phosphorylation, ubiquitination, and methylation (14, 15). Among these, acetylation of core histones (such as H3 and H4) reflects the open chromatin configuration that allows the transcriptional machinery to easily access target genes and thus promote transcription (14, 16). Several groups have reported that polyglutamine aggregates suppress cellular functions at the transcription level, and that this suppression is accompanied by decreased acetylation of core histones. It has been argued that sequestration of major HATs (*e.g.* CBP, PCAF, and TAFII130) underlies this transcriptional suppression (12, 13, 17–19). It is notable that decreased acetylation of core histones and transcriptional dysregulation has been observed not only in polyglutamine disease models, but also in PD, ALS, and AD models (20–22). Unlike polyglutamine disease models, sequestration of transcription factors has not been observed in the PD, ALS, and AD disease models, suggesting that an as-yet unknown mechanism may underlie transcriptional dysregulation in these disorders.

Valosin-containing protein (VCP) is a member of the AAA protein family. VCP has been proposed to function in a variety of physiological processes such as cell cycle regulation, mem-

* This work was supported in part by research grants from the Ministry of Education, Culture, Sports, Science, and Technology of Japan.
[S] The on-line version of this article (available at http://www.jbc.org) contains supplemental Figs. S1–S8.
[1] To whom correspondence should be addressed. Tel.: 81-75-753-7675; Fax: 81-75-753-7676; E-mail: kakizuka@lif.kyoto-u.ac.jp.
[2] The abbreviations used are: UPR, unfolded protein response; VCP, valosin-containing protein; ER, endoplasmic reticulum; AD, Alzheimer disease; PD, Parkinson disease; ALS, amyotrophic lateral sclerosis; HD, Huntington disease; MJD, Machado-Joseph disease; SCA, spinocerebellar ataxia; DLB, dementia with Lewy bodies; TDP, TAR DNA-binding protein; HAT, histone acetyltransferase; AAA, ATPase associated with various cellular activities; ERAD, ER-associated degradation; SOD, superoxide dismutase; IBMPFD, inclusion body myopathy with Paget disease of bone and frontotemporal dementia; GFP, green fluorescent protein; LC/MS/MS, liquid chromatography/tandem mass spectrometry; NLS, nuclear localization signal; NES, nuclear exclusion signal; NI, nuclear inclusion; EF, elongation factor; HA, hemagglutinin; CMV, cytomegalovirus.

brane fusion, ER-associated degradation (ERAD), and ubiquitin-mediated protein degradation (23, 24). We previously identified VCP as a binding partner of MJD proteins with expanded polyglutamine tracts (25). Furthermore, VCP has been shown to colocalize not only with polyglutamine aggregates, but also with Lewy bodies in PD and DLB, SOD1 aggregates in ALS, and dystrophic neurites in AD (25–28). Several lines of evidence have shown that VCP can mediate both aggregate formation and clearance, which is reminiscent of yeast Hsp104, another AAA protein (see references in 29). In addition, by genetic screening using *Drosophila* models of polyglutamine disease, we identified *ter94*, the *Drosophila* homolog of VCP, as a genetic modifier of eye degeneration phenotypes induced by expanded polyglutamine tracts (30). VCP has also been shown to be highly modified by S-thiolation, phosphorylation, and acetylation (31–34).

Recently, about a dozen missense mutations in the human *VCP* gene have been identified as causing inclusion body myopathy with Paget disease of bone and frontotemporal dementia (IBMPFD), an autosomal dominant inherited disease that affects multiple tissues, including muscle, bone, and the cerebral cortex (35–39). Although it is now known that VCP is critically involved in the pathogenesis of several types of human disorders, including neurodegeneration, the detailed molecular mechanisms mediated by VCP in neurodegenerative disorders remain to be elucidated.

EXPERIMENTAL PROCEDURES

Antibodies—Polyclonal antibodies against VCP were developed in our laboratory and described previously (25, 40). The anti-FLAG antibodies (M2 and M5) were obtained from Sigma; anti-actin antibody from Chemicon; anti-histone H3, H4, acetyl-histone H3 (for acetylated Lys-9 and Lys-14), and acetyl-histone H4 (for acetylated Lys-5) antibodies from Upstate Cell Signaling. Anti-GFP and anti-HA antibodies are from Nacalai and Roche, respectively.

Cell Cultures and Transfection—HEK293, NIH3T3, and MCF7 cells were maintained in Dulbecco's modified Eagle's medium (DMEM) (high glucose) with 10% fetal bovine serum. PC12 and its derivative cells were maintained on type 4 collagen-coated culture dishes in DMEM (low glucose) with 10% fetal bovine serum and 5% horse serum with or without 0.5 μg/ml tetracycline. PC12 cell lines expressing wild-type and mutant VCPs under the tet-off promoter were established following a standard procedure as described previously (40). S2R+ cells (41) were maintained in Schneider's *Drosophila* medium with 10% fetal bovine serum. When needed, cells were transfected with expression plasmids using Lipofectamine Plus, Lipofectamine 2000TM, or Cellfectin (Invitrogen).

Construction of Expression Vectors—The full-length VCP cDNAs were subcloned into the pEGFP-N3 vector. The cDNAs for VCP mutants, in which Ser-612 and Thr-613, and Lys-614 were replaced to Asp or Ala, Glu or Ala, and Gln or Ala, respectively, were generated using a site-directed mutagenesis kit (Stratagene). NLS- or NES-coding oligonucleotides were inserted in-frame between the start codon and VCP cording regions. To generate *Drosophila* cell expression vectors, VCP-GFP, FLAG-ter94, and HA-Q79 were subcloned into the pUAST vector. pHrD-Luc was a gift from Drs. Kanda and Mori and contains the human rRNA promoter region spanning −410 to +314 bp (42). pRrD-Luc was constructed by inserting the rat rRNA promoter region spanning −169 to +73, into pGL3-basic vector (Promega).

Quantification of Cultured Cells with Reduced Histone Acetylation—Intensities of immunostaining of acetylated histones were quantified using Image Pro Plus 5.1 software (Media Cybernetics). For each experiment, we evaluated at least 100 cells. When the intensity of the measured cell was more than 25% below the average of control cells, we estimated this cell as having reduced histone acetylation.

Quantification of Cells with Retracted Neurites—PC12 cells with retracted neurites were scored by counting GFP-positive cells in which the neurite lengths were shorter than the cell diameter. For each experiment, we evaluated 100–200 cells. In the figures, the mean values of duplicate experiments are presented, and error bars are included.

Immunocytochemical Analyses—Fixed cells were permeabilized with 0.5% Triton X-100 buffer (0.5% Triton X-100, 20 mM HEPES, 50 mM NaCl, 3 mM $MgCl_2$, and 0.3 M sucrose) for 10 min at room temperature and blocked with blocking buffer (0.1% bovine serum albumin and 0.1% skim milk in phosphate-buffered saline) for 1 h. Cells were then incubated overnight at 4 °C with primary antibodies. Subsequently, cells were treated with Alexa Fluor 488, 546, or 647 secondary antibodies (Invitrogen). DNA was counterstained with TOTO-3 (Invitrogen). Images were taken with a LSM510 confocal microscope (Zeiss).

LC/MS/MS Analyses—Mammalian cell lines such as HEK293T cells were transfected with an expression vector for FLAG-VCP with or without an expression vector for Q79-GFP. Then, FLAG-VCP was immunoprecipitated and was separated by SDS-PAGE. Next, the samples were excised from the gels and were treated with trypsin. The tryptic-digested peptides were analyzed by LC/MS/MS (Waters, 2795 separation module/Thermo Finnigan, LCQ Deca XP plus) (34).

[^{35}S]Methionine/Cysteine Metabolic Labeling—Differentiated PC12 cells were incubated for 30 min in methionine/cysteine-free medium, then labeled for 30 min with 25 μCi of [^{35}S]methionine/cysteine (37 TBq/mmol) (GE Healthcare) in methionine/cysteine-free medium supplemented with 50 ng/ml of NGF in the medium. Ten micrograms of protein from the lysate was subjected to trichloroacetic acid preparation. Incorporated radio counts were measured by a liquid scintillation counter.

Q64C Transgenic Mice—The Q79C mice that we had previously created could not be bred due to very severe ataxia (7), but we recently established new polyglutamine transgenic mice, which express an HA-tagged C-terminal portion of MJD protein with 64 glutamine repeats (Q64C) in Purkinje cells by using the *L7* gene. In one mouse, the transgene integrated into the X chromosome, and we referred to this mouse as Q64C mouse. Thus, the female transgenic mice showed very mild ataxia, probably due to lyonization, and were breedable. We could observe two types of Purkinje cells in female cerebellum: cells with atrophic morphologies that expressed Q64C, and cells with normal morphologies, which did not express Q64C.

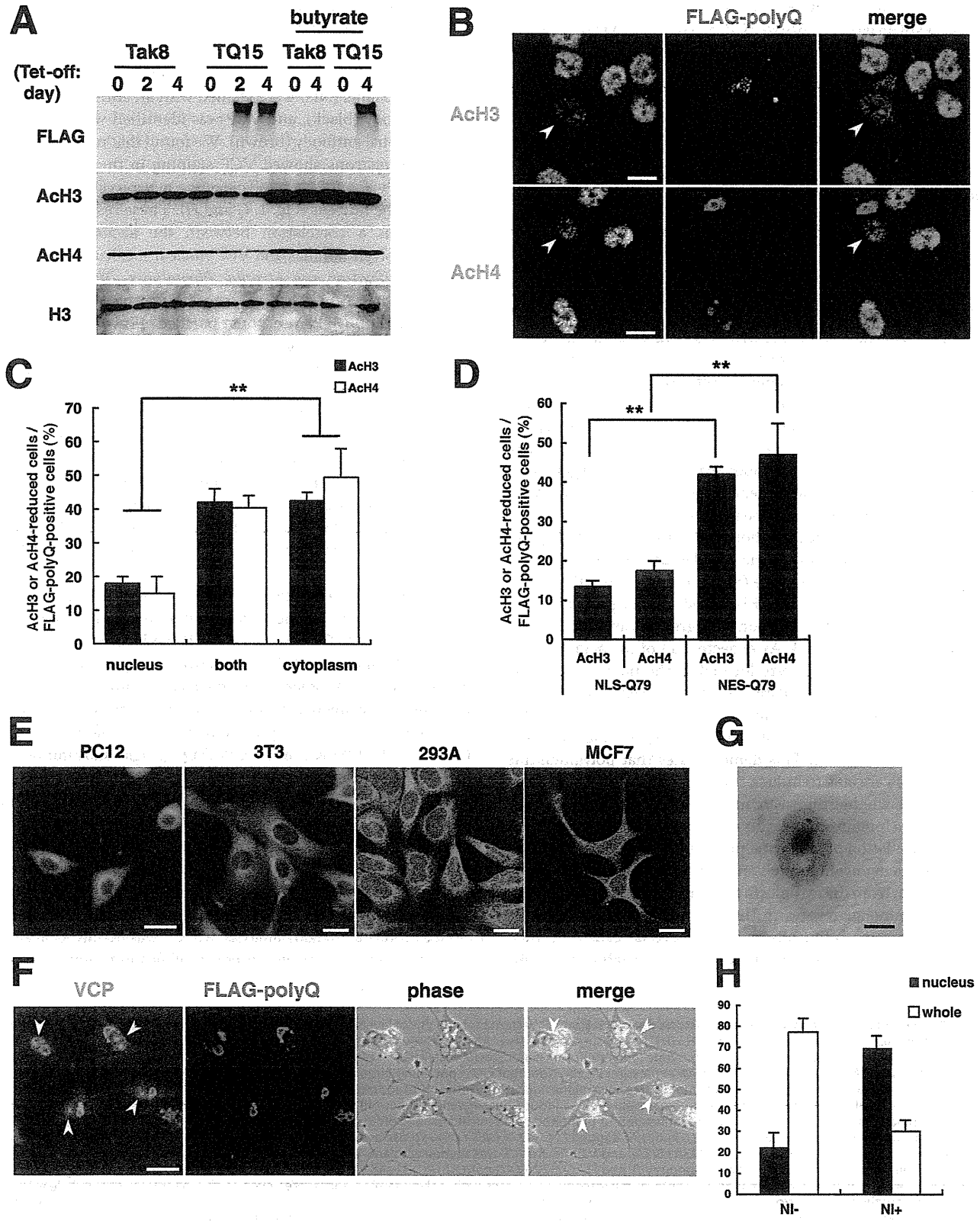

Transgenic Flies—Transgenic flies were created as described previously (30). Genotypes were the followings: GMR-Gal4/+ (+), GMR-Gal4/+; UAS-wtVCP/+ (wtVCP), GMR-Gal4/+; GMR-FlagQ92/+ (Q92), and GMR-Gal4/+; GMR-FlagQ92/UAS-wtVCP (Q92/wtVCP).

Statistical Analysis—Each experiment was conducted at least three times with consistent results. The gel or blot representative of each experiment is presented. The statistical significance was analyzed using Student's *t* test.

RESULTS

Polyglutamine Aggregates, VCP Nuclear Translocation, and Histone Deacetylation—We had previously established a PC12 cell line (TQ15 cells) expressing FLAG-tagged 79-glutamine repeats (Q79) under the control of the tet-off promoter (40). Western blot analysis clearly demonstrated that Lys-9 and Lys-14 of H3 and Lys-5 of H4 were deacetylated after the expression of Q79 in a time-dependent manner (Fig. 1*A*). Addition of butyrate, an inhibitor of histone deacetylases, dramatically recovered or even enhanced the acetylation of histones H3 and H4, which was indistinguishable between cells with or without polyglutamine aggregates (Fig. 1*A* and supplemental Fig. S1). These observations fit well with the idea that expanded polyglutamine tracts contribute to enhancement of histone deacetylation rather than to diminishment of histone acetylation.

Surprisingly, significantly more cells with cytoplasmic aggregates showed a decrease in H3 and H4 acetylation than cells with nuclear aggregates alone (Fig. 1, *B* and *C*). We then transiently expressed NLS- or NES-tagged Q79 in parental PC12 cells and examined the location of aggregates and the acetylation levels of H3 and H4. As expected, all of the aggregates of NLS-Q79 or NES-Q79 were located in the nucleus or in the cytoplasm, respectively (data not shown). Significantly more cells expressing NES-Q79 showed a decrease in H3 and H4 acetylation than cells expressing NLS-Q79 (Fig. 1*D* and supplemental Fig. S2). This demonstrates that polyglutamine aggregates were able to induce core histone deacetylation, irrespective of whether they were nuclear or cytoplasmic.

We have long examined the relationship between VCP and the accumulation of abnormal proteins such as those containing expanded polyglutamines and noticed that VCP changes its localization from the cytoplasm to the nucleus even in cells with polyglutamine aggregates in the cytoplasm (Fig. 1, *E* and *F*), which was most often observed in neuronal cells. We then examined brain sections from our recently established Q64C mice and MJD patients. In Purkinje cells from normal mice, VCP was distributed diffusely throughout the cell. In contrast, VCP was mainly localized within the nucleus in the Q64C-expressing atrophic Purkinje cells of Q64C mice (supplemental Figs. S3 and S4). In the brain sections of MJD patients, nuclear inclusions (NIs) were stained with an anti-1C2 monoclonal antibody (black), and VCP was identified with an anti-VCP polyclonal antibody (brown). We found that nearly 80% of NI-positive neurons showed VCP staining in the nucleus. In contrast, only about 20% of NI-negative neurons showed VCP staining in the nucleus (Fig. 1, *G* and *H*). These results showed that there is a correlation between the accumulation of expanded polyglutamines and VCP nuclear localization.

VCP Modification and Atrophic Phenotypes—We have previously shown that VCP is highly modified by phosphorylation and acetylation (34). We thus purified FLAG-VCP from HEK293T cells expressing expanded polyglutamine tracts, analyzed it by LC/MS/MS, and found that three sequential amino acids, Ser-612, Thr-613, and Lys-614, were modified simultaneously by phosphorylation, phosphorylation, and acetylation, respectively (Fig. 2). These sequential modifications were not observed in VCP purified from cells expressing normal lengths of polyglutamines. The same sequential modifications were observed, although less frequently, in purified FLAG-VCP from MG132-treated cells (34). In the absence of MG132 treatment, these sequential modifications were not detected by LC/MS/MS analysis.

To elucidate the biological significance of these VCP modifications, we introduced amino acid substitutions mimicking these modifications into VCP. Ser-612, Thr-613, and Lys-614 were substituted with aspartic acid (D) (a negatively charged amino acid), glutamic acid (E) (another negatively charged amino acid), and glutamine (Q) (an uncharged amino acid), respectively, in various combinations. The resulting substituents were referred to as: VCP(**D**TK), VCP(S**E**K), and VCP(ST**Q**) (single substitutions); VCP(**DE**K) (double substitution); and VCP(**DEQ**) (triple substitution). In addition, alanine was introduced as several control substitutions. The resulting substituents were referred to as: VCP(AAK), VCP(AAQ), VCP(DEA), and VCP(AAA). These substituents, as well as wild-type VCP (wtVCP), were expressed as GFP-tagged proteins in PC12 cells. We were thus able to examine these exogenously expressed VCPs with live cell-imaging analysis as well as confocal imaging analysis. wtVCP was mainly localized in the cytoplasm. However, several modification-mimic VCPs

FIGURE 1. **Polyglutamine aggregates and histone deacetylation.** *A*, Western blot analysis of levels of FLAG-tagged Q79 (*FLAG*), acetylated histones H3 and H4 (*AcH3* and *AcH4*, respectively), and histone H3 (*H3*) before and 2 and 4 days after the removal of tetracycline from TQ 15 cells (*TQ15*) and parental PC12 cells (*Tak8*), in the absence and presence of 2.5 mM butyrate (*butyrate*). *B*, immunocytochemical analysis of acetylated histones H3 (*AcH3*) and H4 (*AcH4*) in PC12 cells transfected with FLAG-tagged Q79 (*FLAG-polyQ*) expression vector. Note that cells containing large polyglutamine aggregates (*arrowheads*) showed a clear decrease in acetylated histone levels. Merged images are shown in the *right panels* with indicated colors. *Bars*, 10 μm. *C*, quantification of immunocytochemical analysis in *B*. Cytoplasmic polyglutamine aggregates appeared to induce deacetylation of core histones (AcH3 and AcH4) in more cells than did nuclear polyglutamine aggregates. **, $p < 0.01$. *D*, quantification of immunocytochemical analyses of acetylated histones H3 (*AcH3*) and H4 (*AcH4*) in PC12 cells transfected with NLS-tagged FLAG-Q79 (*NLS-Q79*) or NES-tagged FLAG-Q79 (*NES-Q79*) expression vectors. **, $p < 0.01$. *E*, immunocytochemical analysis of endogenous VCP in PC12, NIH3T3 (*3T3*), HEK293A (*293A*), and MCF7 cells. VCP was stained with anti-VCP (*green*) and imaged by confocal microscopy. *Bars*, 20 μm. *F*, immunocytochemical analysis of endogenous VCP and FLAG-Q79 (*FLAG-polyQ*) in PC12 cells. VCP and FLAG-Q79 were stained with anti-VCP (*green*) and anti-FLAG (*red*), respectively, and imaged by confocal microscopy. PC12 cells with polyglutamine aggregates even in the cytoplasm showed clear VCP accumulation in the nucleus (*arrowheads*). *Bar*, 20 μm. *G*, immunohistochemical analysis of VCP in neurons from MJD patients. Brain sections from MJD patients were stained with anti-VCP (*brown*) and anti-1C2 for expanded polyglutamine (50) (*black*), and signals were visualized by the ABC method. *Bar*, 5 μm. *H*, quantification of VCP localization in the neurons from MJD patients in *G*. At least 200 neurons were imaged randomly and scored for localization of endogenous VCP in either nuclear inclusion-positive or -negative neurons.

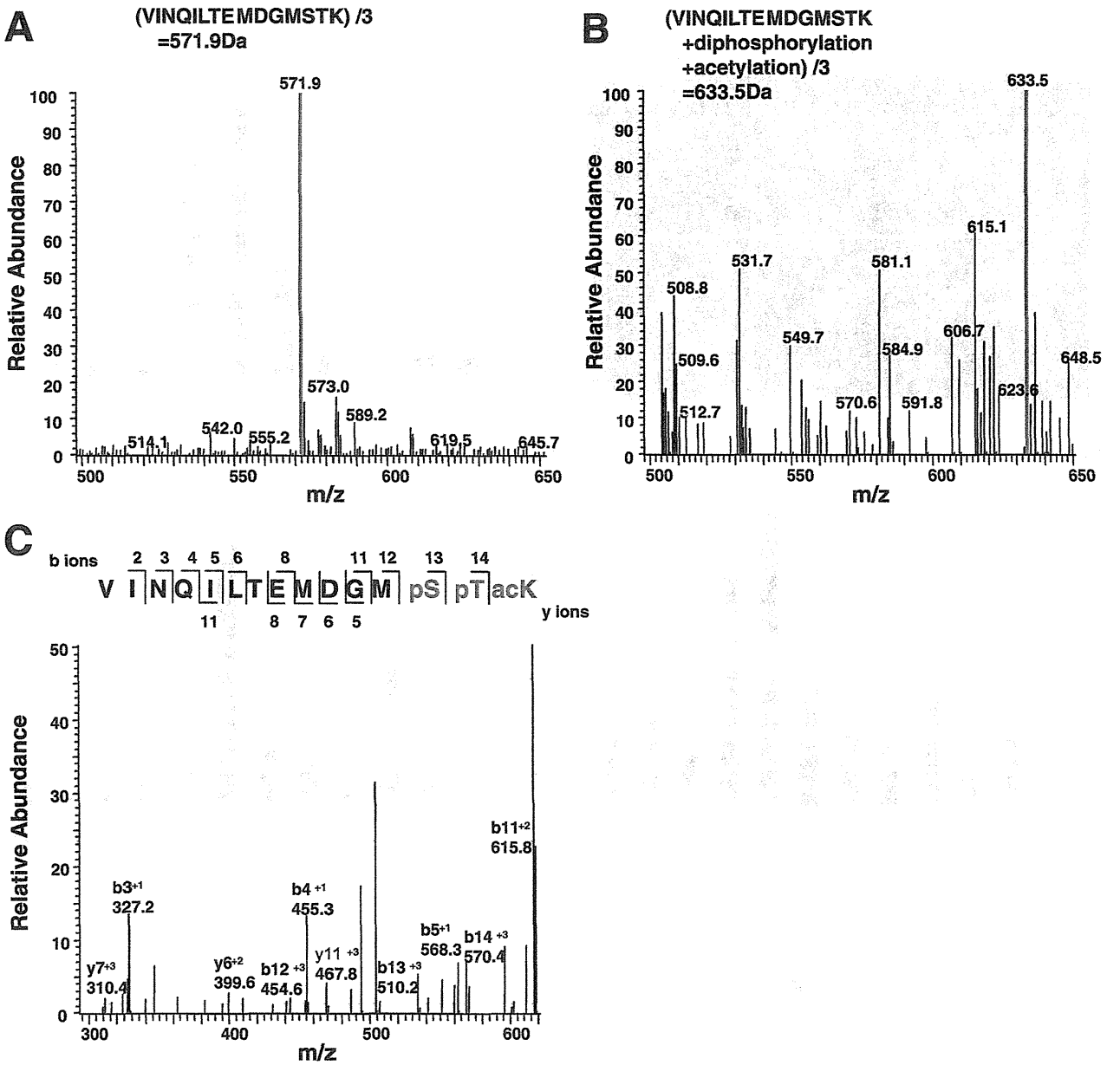

FIGURE 2. **Detection of modified Ser-612, Thr-613, and Lys-614 in VCP by LC/MS/MS analysis.** *A*, exclusive detection of the peptide from Val-600 to Lys-614 with molecular mass of 1,715.7 Da (571.9 Da ×3) in VCP recovered from non-treated HEK293T cells. From the molecular mass, two oxidized methionines were predicted, but any phosphorylation or acetylation site was not predicted in this peptide. *B*, detection of the modified peptide from Val-600 to Lys-614 with molecular mass of 1,900.5 Da (633.5 Da ×3) in VCP recovered from expanded polyglutamine-expressing HEK293T cells. From the molecular mass, one oxidized methionine, two phosphorylation sites, and one acetylation site were predicted in this peptide. *C*, an analytical data of LC/MS/MS with VCP recovered from expanded polyglutamine-expressing HEK293T cells. A tandem mass spectrum of the tryptic peptide with molecular mass of 1,900.5 Da (633.5 Da ×3) from immunoprecipitated FLAG-VCP shows detection of Ser-612, Thr-613, and Lys-614 being phosphorylated, phosphorylated, and acetylated, respectively. The MS/MS spectrum of the peptide with molecular mass of 633.5 Da ×3 in *B* was searched against a database constructed from the reported human VCP sequence utilizing SEQUEST program. Search parameters were modified to consider possible phosphorylation (+80) at all serine, threonine, or tyrosine residues, possible oxidation (+16) at methionine, and possible acetylation (+42) at lysine. Matched b or y ions via automatic computational interpretation are displayed as numbers in the sequence panel and the attribution of the strong peaks among them are indicated in the spectrum. Significant peaks that match to theoretical peaks interpreted by MS-Product are shown with numbers of the mass in the spectrum.

localized in the nucleus with different degrees. VCP(DEQ) was most often localized within the nucleus, followed by VCP(DEA) and VCP(DEK) (Fig. 3, *A* and *B*). VCP (AAA), VCP(AAQ), and VCP(AAK) were mostly excluded from the nucleus; less than 5% of transfected cells showed nuclear localization of these substituents (Fig. 3, *A* and *B*).

Surprisingly, 5 days after transfection, ~30% of the PC12 cells expressing VCP(DEQ) showed shrinkage of cell volume with neurite retraction (Fig. 3, *A* and *C*). We called this an "atrophic phenotype". The atrophic phenotype was most prominent in cells expressing VCP(DEQ), followed by VCP(DEA) and VCP(DEK) (Fig. 3*C*), and it was exactly correlated with

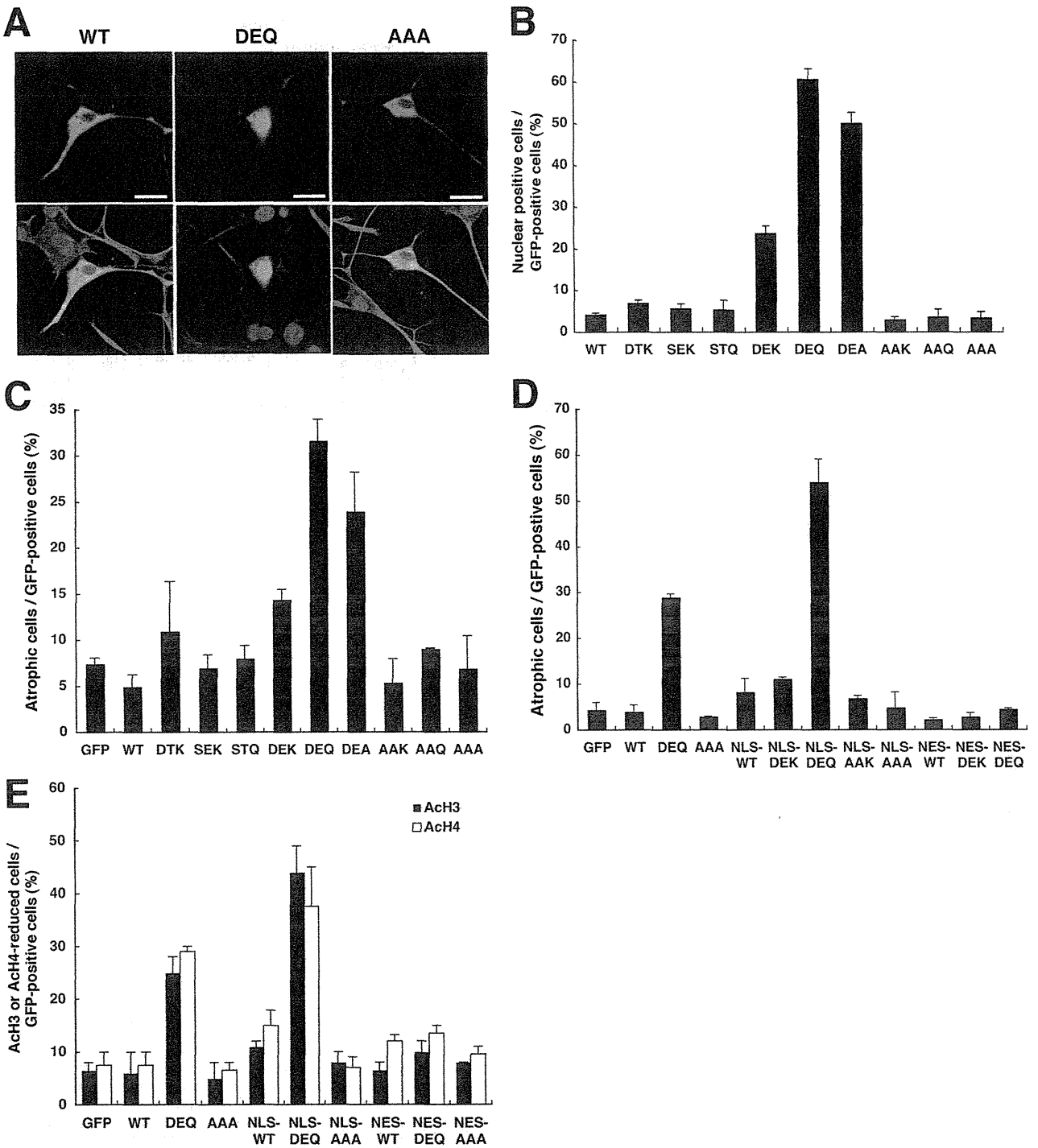

FIGURE 3. **Phenotypes of PC12 cells induced by modification-mimic forms of VCP.** *A*, immunocytochemical analysis of PC12 cells expressing GFP-tagged wild-type VCP, VCP(DEQ), and VCP(AAA). VCP(DEQ), but not wild-type VCP or VCP(AAA), localized within the nucleus. Four days after transfection, PC12 cells were fixed and stained with anti-GFP (*green*), anti-β-tubulin (*red*), and TOTO-3 (*blue*). PC12 cells expressing VCP(DEQ) showed retracted neurites and were small in size (atrophic phenotype). *Bars*, 20 μm. *B*, quantification of GFP-tagged wild-type and various forms of VCP localization in PC12 cells. At least 200 GFP-positive cells were imaged randomly and scored for the nuclear localization of GFP signals. *C*, quantification of atrophic phenotypes in PC12 cells expressing GFP-tagged wild-type and various forms of VCP. At least 200 GFP-positive cells were imaged randomly and scored for atrophic phenotypes. *D*, quantification of atrophic phenotypes in PC12 cells expressing GFP-tagged wild-type or various forms of VCP, some of which were also tagged with NLS or NES. At least 200 GFP-positive cells were imaged randomly and scored for atrophic phenotypes. *E*, quantification of immunocytochemical analysis for decreased histone acetylation in cells expressing GFP-tagged wild-type or various forms of VCP. At least 100 GFP-positive cells were imaged randomly and scored for decreased histone acetylation.

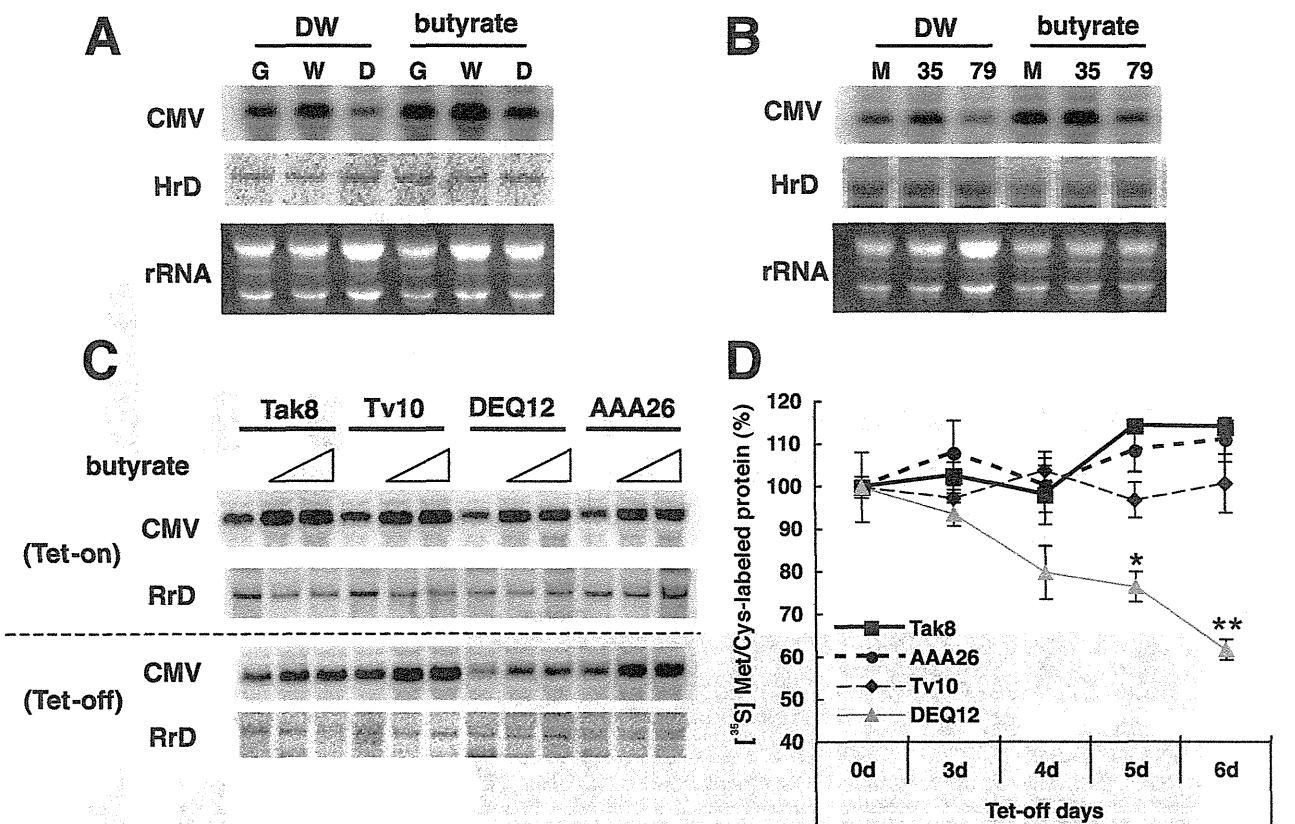

FIGURE 4. **VCP modification and suppression of transcription and protein synthesis.** *A*, Northern blot analysis of RNAs transcribed from CMV and human rRNA promoters in HEK293T cells. HEK293T cells were transfected with pCMV-luciferase 2 (*CMV*) and pHrRNA-luciferase (*HrD*), together with the expression vector for GFP (*G*), VCP-GFP (*W*), or VCP(DEQ)-GFP (*D*). Three days after transfection, RNAs were extracted and analyzed by Northern blot using radiolabeled luciferase or luciferase 2 cDNA as a probe. *B*, Northern blot analysis of RNAs transcribed from CMV and human rRNA promoters in HEK293T cells. HEK293T cells were transfected with pCMV-luciferase 2 (*CMV*) and pHrRNA-luciferase (*HrD*), together with an empty expression vector (*M*) or an expression vector for Q35 (*35*) or Q79 (*79*). Three days after transfection, RNAs were extracted and analyzed by Northern blot using radiolabeled luciferase or luciferase 2 cDNA as a probe. *C*, Northern blot analyses of RNAs transcribed from the CMV promoter in PC12 cells. Parental PC12 cells (Tak8) or PC12 cells expressing GFP-tagged wild-type VCP (Tv10), VCP(DEQ) (DEQ12), or VCP(AAA) (AAA26) under the control of the tet-off promoter were transfected with pCMV-luciferase 2 (*CMV*) together with pRrRNA-luciferase (*RrD*). One day after transfection, different amounts of butyrate (1 and 2.5 mM) were added in the presence (Tet-on) or absence (Tet-off) of tetracycline. Three days after transfection, RNAs were extracted and analyzed. The same blots were sequentially probed with radiolabeled luciferase 2 and luciferase cDNAs. *D*, measurement of *de novo* protein synthesis in Tak8, Tv10, DEQ12, and AAA26 cells. In the presence of tetracycline (0d) or 3, 4, 5, 6 days after it was removed, cells were labeled with [^{35}S]Met/Cys for 30 min and lysed. Incorporated radio counts were measured as described under "Experimental Procedures." Experiments were performed in duplicate, and mean values and error bars are presented. **, $p < 0.01$.

their nuclear translocation (Fig. 3, *B* and *C*). More cells expressing VCP(DEQ) showed an atrophic phenotype with increasing time, but remained alive even 7 days after transfection (data not shown). We could observe very little of the atrophic phenotype in cells expressing wtVCP (less than 5%).

We next sought to determine the cause of the atrophic phenotype, whether it was VCP nuclear localization, VCP amino acid substitution, or both. To this end, we expressed NLS- and NES-tagged wtVCP and several substituents in PC12 cells, and examined the phenotypes. All of the NLS-tagged VCPs translocated to the nucleus, and all of the NES-tagged VCPs stayed in the cytoplasm (data not shown). NLS-VCP(DEQ) induced the atrophic phenotype most frequently (more than 50% of cells) (Fig. 3*D*). The expression of other NLS-tagged VCPs (wtVCP, VCP(DEK), VCP(AAK), and VCP(AAA)) either did not result in or only marginally increased the atrophic phenotype (Fig. 3*D*). Conversely, NES-VCP(DEQ) did not result in the atrophic phenotype (Fig. 3*D*). These data demonstrate that both the modifications and the nuclear localization of VCP were necessary for the atrophic phenotype. Taken together, the above results suggested that modified VCP mediates a signal from the cytoplasm to the nucleus, leading to histone deacetylation. Indeed, deacetylations of H3 and H4 histones were observed in cells expressing VCP(DEQ) and NLS-VCP(DEQ), but not or only marginally in cells expressing wtVCP or VCP(AAA), even in the presence of NLS (Fig. 3*E* and supplemental Fig. S5).

VCP Modification and the Suppression of Transcription and Protein Synthesis—We next examined whether VCP(DEQ) expression could suppress steady-state mRNA levels in a transient transfection assay. For this experiment, we prepared an expression vector for luciferase RNA with the rat or human ribosomal RNA (rRNA) promoter (pRrD-Luc or pHrD-Luc, respectively), as an internal transfection control. Northern blot analysis revealed that luciferase RNA levels from both of the rRNA promoters were not affected by the addition of α-amanitin (an inhibitor of RNA polymerase II) or butyrate, or by wtVCP or VCP(DEQ) expression. However, the addition of actinomycin D (an inhibitor of RNA polymerase I) completely

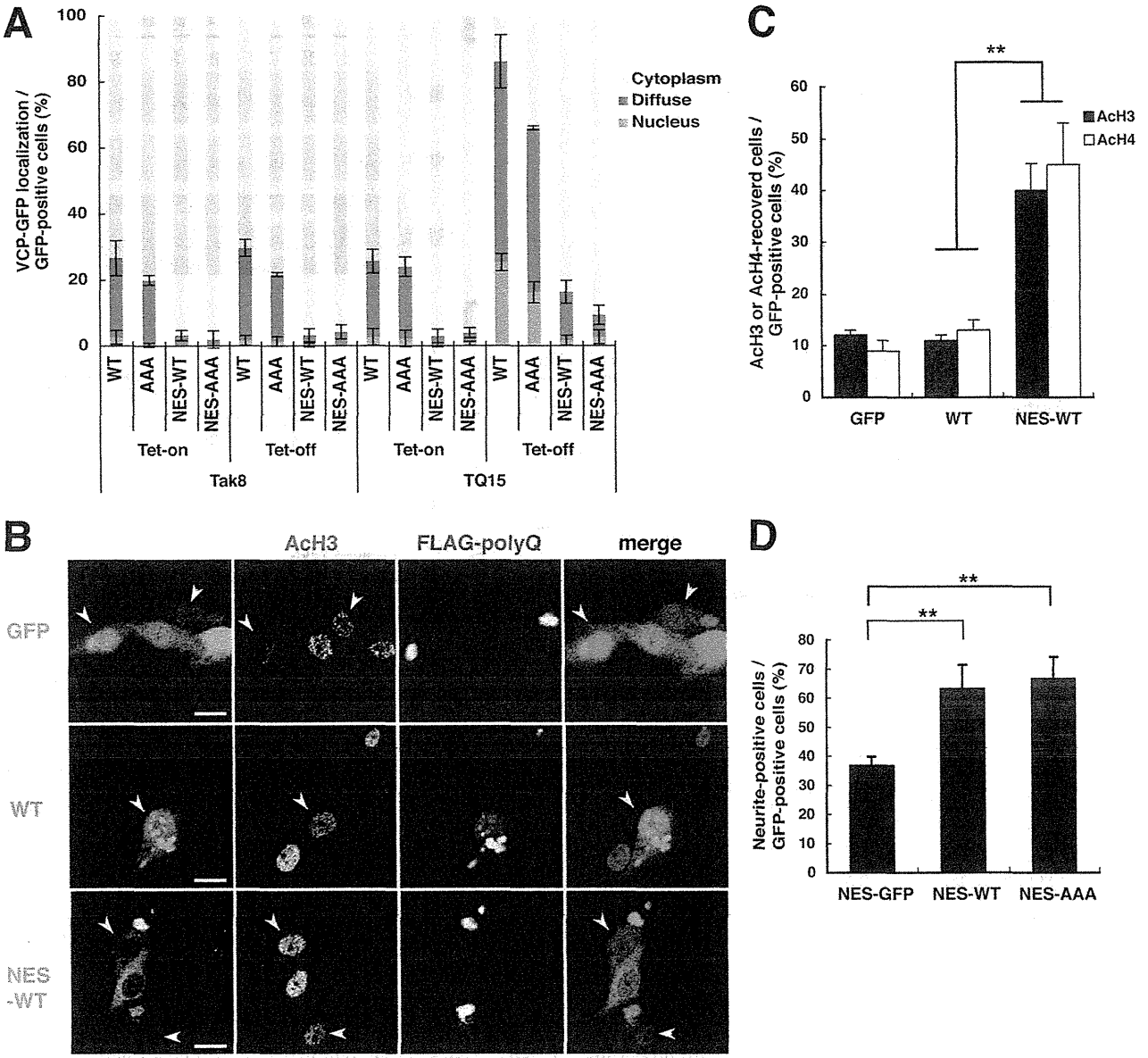

FIGURE 5. **Prevention of polyglutamine-induced histone deacetylation and neurite retraction by NES-VCPs.** *A*, quantification of intracellular localization of GFP-tagged wild-type or various forms of VCP in parental PC12 cells (Tak8) and PC12 cells expressing FLAG-Q79 under the control of the tet-off promoter (TQ15). TQ15 cells were transfected with GFP-tagged wild-type or various forms of VCP. One day after the transfection, tetracycline was removed from the media. Three days after removal of tetracycline, live cells were imaged for GFP signals. At least 200 GFP-positive cells were imaged randomly and scored. *B*, immunocytochemical analysis of TQ15 cells, transfected with GFP, GFP-tagged wild-type VCP (*WT*), or GFP- as well as NES-tagged wild-type VCP (*NES-WT*). One day after transfection, tetracycline was removed from the medium. Four days after removal of tetracycline, cells were fixed and stained with anti-GFP, anti-AcH3, and anti-FLAG. *Arrowheads*: cells containing polyglutamine aggregates. Merged images are also shown in the *right panels* with indicated colors. *Bars*, 15 μm. *C* and *D*, quantification of cells with recovered histone H3 acetylation levels (*C*) or neurite-positive cells (*D*) among GFP-positive PC12 cells expressing FLAG-Q79 under the same conditions as in *B*. At least 100 (*C*) and 200 (*D*) cells were imaged randomly and scored. **, $p < 0.01$.

blocked the luciferase RNA expression (Fig. 4, *A* and *B*, and supplemental Fig. S6).

We then investigated whether VCP(DEQ) affected the promoter activities of different genes transcribed by RNA polymerase II. HEK293T cells were transfected with expression vectors for GFP, wtVCP-GFP, or VCP(DEQ)-GFP, along with pHrD-Luc and a well-used vector that expresses luciferase 2. We examined levels of luciferase 2 mRNA by Northern blot and found that luciferase 2 mRNA from all of the tested promoters (*e.g.* those from the cytomegalovirus (CMV) and *EF-1α* genes) was suppressed by the expression of VCP(DEQ)-GFP, but not wtVCP-GFP (Fig. 4*A*, and not shown). Interestingly, this suppression was not fully ameliorated by the addition of butyrate (Fig. 4*A*). Similar decreases in mRNA levels were observed in cells transfected with the Q79 expression vector, but not the Q35 expression vector or empty vector (Fig. 4*B*). Again, this suppression was not fully ameliorated by the addition of butyrate (Fig. 4*B*).

A

600	615	
VINQILTEMDGMSTKK		*Homo sapiens*
VINQILTEMDGMSTKK		*Rattus norvegicus*
VINQILTEMDGMSTKK		*Mus musculus*
VINQILTEMDGMSIKK		*Xenopus laevis*
VINQILTEMDGMGAKK		*Drosophila melanogaster* (ter94)
VINQVLTEMDGMNAKK		*Caenorhabditis elegans* (Cdc48.1)
VLNQLLTEMDGMNAKK		*Arabidopsis thaliana* (Cdc48p)
V-NQLLTEMDGMNAKK		*Saccharomyces cerevisiae* (Cdc48p)

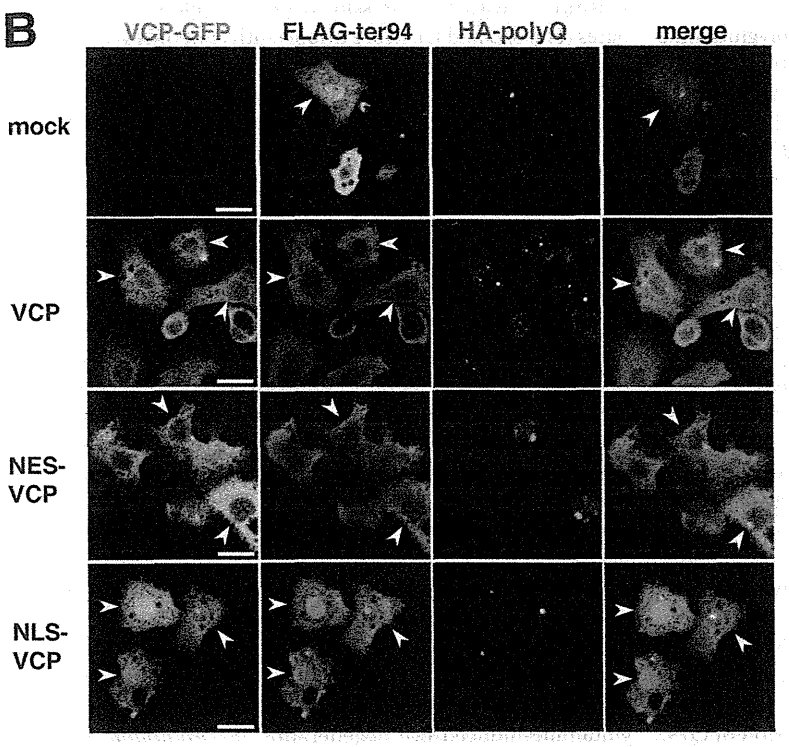

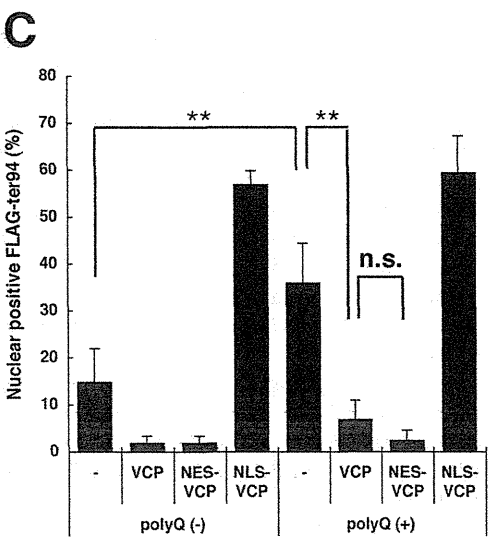

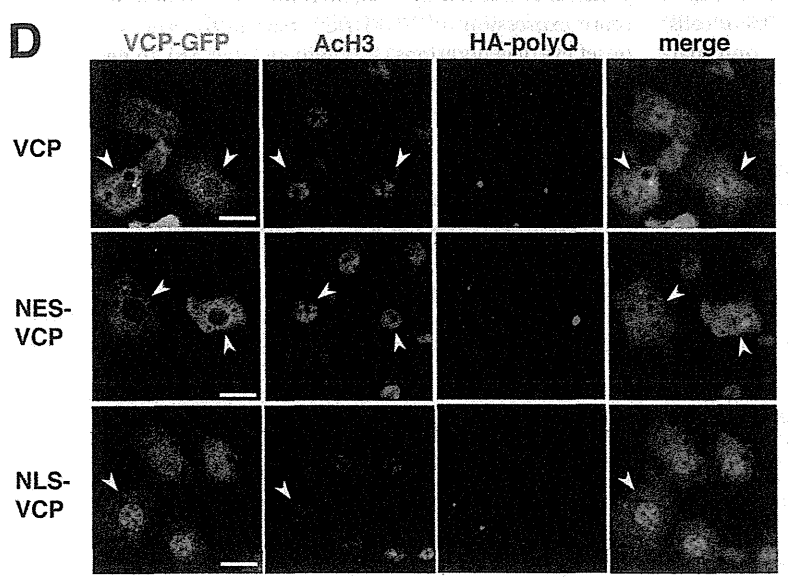

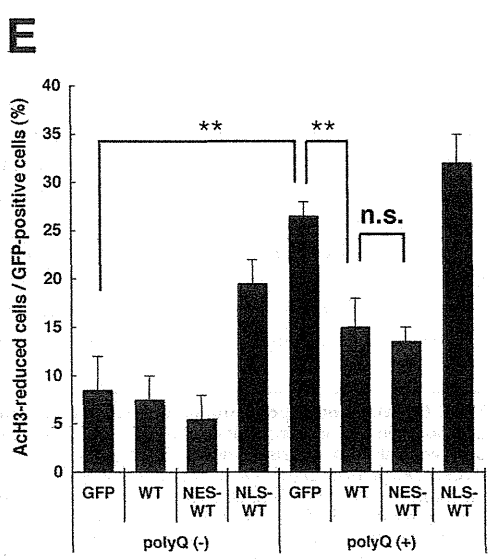

We then performed a similar set of experiments using Tak8 (parental PC12 cells), Tv10 (PC12 cells expressing GFP-tagged wtVCP under the control of the tet-off promoter)(43), DEQ12 (PC12 cells expressing GFP-tagged VCP(DEQ) under the control of the tet-off promoter), and AAA26 cells (PC12 cells expressing GFP-tagged VCP(AAA) under the control of the tet-off promoter) (supplemental Fig. S7). Consistent with the results from the HEK293T cells, luciferase 2 mRNA levels from the CMV promoter were suppressed in DEQ12 cells but not in Tak8, Tv10, or AAA26 cells 3 days after the removal of tetracycline. Again, this suppression was not fully ameliorated by the addition of butyrate (Fig. 4*C*).

The above results indicate that expanded polyglutamine expression induced VCP modifications, which in turn induced suppression of transcription from promoters transcribed by RNA polymerase II but not RNA polymerase I. Thus, we expected *de novo* protein synthesis to be reduced. To investigate this possibility, we examined the levels of *de novo* protein synthesis in Tak8, Tv10, DEQ12, and AAA26 cells by measuring [^{35}S]methionine/cysteine incorporation into newly synthesized proteins. Indeed, we confirmed that *de novo* protein synthesis was significantly decreased in DEQ12 cells, but not in Tv10 or AAA26 cells 5 and 6 days after removal of tetracycline (Fig. 4*D*).

Prevention of Polyglutamine-induced Phenotypes by NES-VCPs in PC12 Cells—We next examined the potential dominant-negative effects of VCP(AAA) on endogenous VCP. In Tak8 cells (parental PC12 cells), tetracycline removal did not affect the intracellular distribution of GFP-tagged wtVCP, VCP(AAA), NES-wtVCP, or NES-VCP(AAA) (Fig. 5*A*). Approximately 20% of cells with GFP signals in the nucleus were expressing wtVCP or VCP(AAA); very few cells with nuclear GFP were expressing NES-wtVCP or NES-VCP(AAA). Similar expression patterns were observed in TQ15 cells (PC12 cells expressing FLAG-Q79 under the control of the tet-off promoter)(40) in the presence of tetracycline. However, tetracycline removal from TQ15 cells, resulting in expression of Q79, induced nuclear translocation of both wtVCP (~80% of cells) and VCP(AAA) (~70% of cells) (Fig. 5*A*). In contrast, only marginal nuclear translocation of NES-wtVCP or NES-VCP(AAA) was observed in TQ15 cells 4 days after removal of tetracycline (Fig. 5*A*). Consistent with these results, overexpression of NES-wtVCP or NES-VCP(AAA) was able to suppress the expanded polyglutamine-induced deacetylation of histone H3 (Fig. 5, *B* and *C*, and not shown), as well as neurite retraction (Fig. 5*D*).

Prevention of Polyglutamine-induced Phenotypes by wtVCP in Drosophila—It is notable that Ser-612 and Thr-613 are changed to Gly and Ala, respectively, in ter94, *Drosophila* VCP (Fig. 6*A*). This suggested the lack of kinases for the phosphorylation of these serine and threonine in *Drosophila*. Given that Ser-612 and Thr-613 of mammalian VCP could not be phosphorylated in *Drosophila*, it was interesting to see whether mammalian VCP was also able to translocate into the nucleus in *Drosophila* cells in the presence of polyglutamine aggregates. We thus examined this possibility using S2R+ cells (41), a *Drosophila* cell line, by expressing FLAG-ter94 with HA-tagged Q92 (Q92). In the absence of Q92 expression, ter94 resided mainly in the cytoplasm. In the presence of Q92 aggregates, ter94 traslocated into the nucleus (Fig. 6*B*, *uppermost panels*). However, wtVCP as well as NES-wtVCP stayed in the cytoplasm, even with co-expression of ter94 in cells with Q92 aggregates (Fig. 6, *B* and *C*). More importantly, not only NES-wtVCP but also wtVCP significantly prevented ter94 nuclear translocation in cells with Q92 aggregates (Fig. 6, *B* and *C*). Consistent with this, in cells expressing wtVCP or NES-wtVCP, acetylation levels of core histones were also significantly recovered even with Q92 aggregates (Fig. 6, *D* and *E*). It is noteworthy that in *Drosophila* S2R+ cells, NLS-VCP itself could induce deacetylation of core histones with its nuclear localization (Fig. 6, *D* and *E*), although this was only marginally observed in mammalian cells (Fig. 3*E*).

We previously showed that overexpression of ter94, *Drosophila* VCP, enhanced polyglutamine-induced eye degenerations (30). It was evident, in contrast, that overexpression of mammalian VCP (wtVCP) in fly eyes clearly suppressed eye degenerations when co-expressed with expanded polyglutamines, without apparently affecting the levels of polyglutamine aggregates (Fig. 7, *A* and *B*). In degenerated eyes, endogenous ter94 located in the nucleus (Fig. 7*C*). In cured eyes, however, overexpressed wtVCP and ter94 predominantly resided in the cytoplasm (Fig. 7*C*), and acetylation levels of core histones were significantly recovered (Fig. 7, *D* and *E*). These results, altogether, indicated that in *Drosophila* cells wtVCP could function in a way similar to NES-wtVCP in mammalian cells, and thus overexpression of wtVCP could mitigate polyglutamine-induced eye degeneration in *Drosophila*. Furthermore expression of VCP(DEQ) itself in fly eyes induced late onset eye degenerations (supplemental Fig. S8). In degenerated eyes, clear reductions in acetylation levels of core histones were observed (supplemental Fig. S8).

DISCUSSION

Several reports have shown that expanded polyglutamine expression decreases the acetylation of core histones such as H3 and H4 (12, 13, 17, 19). We first confirmed this observation in our cell culture model of polyglutamine disease (40). Indeed, the experiments presented here using anti-acetylated H3 (for acetylated Lys-9 and Lys-14) and H4 (for acetylated Lys-5) anti-

FIGURE 6. **Prevention of polyglutamine-induced ter94 nuclear translocation and histone deacetylation by wtVCP in *Drosophila* S2R+ cells.** *A*, amino acid alignment of modified residues in VCP among different species. Lys-614 was widely conserved among different species; Ser-612 and Thr-613 were conserved only in mammals. *B*, immunocytochemical analysis of S2R+ cells transfected with FLAG-ter94 and HA-Q79 (HA-polyQ) with or without GFP-tagged wtVCP(VCP), NES-wtVCP(NES-VCP), and NLS-wtVCP(NLS-VCP). FLAG-ter94 was detected with an anti-FLAG M5 antibody, Q79 with an anti-HA antibody, VCPs with an anti-GFP antibody. Merged images are also shown in the *right panels* with indicated colors. *White arrowheads* show cells with Q79 aggregates. *Bars*, 10 μm. *C*, quantification of immunocytochemical analysis in *B*. At least 200 FLAG-positive cells were imaged randomly and scored. **, $p < 0.01$. *n.s.*, not significant. *D*, immunocytochemical analysis of S2R+ cells transfected with HA-Q79 (*HA-polyQ*) with GFP-tagged wtVCP (*VCP*), NES-wtVCP (*NES-VCP*), and NLS-wtVCP (*NLS-VCP*). Q79 was detected with an anti-HA antibody, acetyl-H3 (AcH3) with an anti-acetylated histone H3 antibody, VCPs with an anti-GFP antibody. Merged images are also shown in the *right panels* with indicated colors. *White arrowheads* indicate cells with Q79 aggregates. *Bars*, 10 μm. *E*, quantification of immunocytochemical analysis in *D*. At least 100 GFP-positive cells were imaged randomly and scored. **, $p < 0.01$; *, $p < 0.05$; *n.s.*, not significant.